Optics Letters

High-power, low-noise Brillouin laser on a silicon chip

Yingchun Qin,[1,†] Shulin Ding,[1,†] Menghua Zhang,[1] Yunan Wang,[1] Qi Shi,[1] Zhixuan Li,[1] Jianming Wen,[2] Min Xiao,[1,3] and Xiaoshun Jiang[1,*]

[1]National Laboratory of Solid State Microstructures, College of Engineering and Applied Sciences and School of Physics, Nanjing University, Nanjing 210093, China
[2]Department of Physics, Kennesaw State University, Marietta, Georgia 30060, USA
[3]Department of Physics, University of Arkansas, Fayetteville, Arkansas 72701, USA
*Corresponding author: jxs@nju.edu.cn
†These authors contributed equally to this Letter.

Received 1 February 2022; revised 27 February 2022; accepted 27 February 2022; posted 28 February 2022; published 21 March 2022

We realize a chip-based Brillouin microlaser with remarkable features of high power and low noise using a microtoroid resonator. Our Brillouin microlaser is able to output a power of up to 126 mW with a fundamental linewidth down to 245 mHz. Additionally, in the course of Brillouin lasing we observe an intriguing power saturation-like effect, which can be attributed to complex thermo-optic-effect-induced mode mismatch between the pump and Brillouin modes. To have a quantitative understanding of this phenomenon, we develop a model by simultaneously considering Brillouin lasing and the thermo-optic effect occurring in the microcavity. Of importance, our theoretical results match well with experimentally measured data.

https://doi.org/10.1364/OL.455369

Brillouin microlasers [1–4] have emerged as a crucially important approach for designing integrated narrow-linewidth lasers [5–11] which have been further applied for laser gyroscopes [8,12], generation of low-noise microwave signal [8,13] and Brillouin–Kerr soliton microcombs [14], as well as realization of narrow-linewidth Kerr microcombs [15]. So far, Brillouin microlasers have been achieved in various resonator platforms ranging from silica spheres/disks [2,5,6], crystal disks [1,16], silicon nitride microrings [8,10,11], silicon microrings [17], to chalcogenide microrings [18]. Despite these impressive achievements, the achieved output lasing powers are limited to approximately 20 mW [8], because of the Brillouin laser cascade [8,19] as well as the interactions of the stimulated Brillouin scattering (SBS) with other forms of nonlinearities in the microcavity such as four-wave mixing (FWM) [14,20,21] and the thermo-optic effect [22], which adversely constrains their further potential for use in atomic physics and integrated nonlinear photonics.

Here, we report the realization of a chip-based Brillouin microlaser with an output power of up to 126 mW and a fundamental linewidth down to 245 mHz by making use of a microtoroid resonator. We notice that increase of the Brillouin laser output has been demonstrated by employing different transverse mode families for the pump and Brillouin modes [9] or by incorporating Bragg gratings [23] to inhibit the Brillouin lasing cascade. Compared with the silica microdisk resonator [5], the microtoroid resonator [24] enables a larger mode volume and more transverse optical modes, and such a relatively large optical mode volume inversely reduces the thermo-optic effect. Therefore, the optical modes inside the microcavity are able to tolerate much higher power but experience less thermal frequency shift. Inspired by these observations, in this work, we have successfully inhibited the Brillouin laser cascade by using two different high-order optical transverse modes in a microtoroid cavity with relatively large mode volume.

Experimentally, we choose a fiber taper coupled high-Q silica microtoroid resonator [25] with a diameter of ~3.350 mm to produce the Brillouin laser. Since the free spectral range (FSR) is larger than the Brillouin phonon frequency, the system only allows the Brillouin laser to be generated within different transverse mode families, thereby preventing the Brillouin lasing cascade. This non-cascading Brillouin laser operation is schematically illustrated in the spectral diagram of Fig. 1(a). Moreover, the relatively high-density optical modes in the microcavity help to reduce the difficulty in attaining phase matching conditions for the Brillouin laser generation. As a result, Brillouin lasing is observed in almost every FSR around the telecom 1550-nm band.

Figure 2 shows the experimental setup used for the generation and characterization of the Brillouin microlaser. An external-cavity diode laser amplified by an erbium-doped fiber amplifier (EDFA) is used as the pump light for the Brillouin laser generation. The pump light is locked to the cavity mode [pump mode in Fig. 1(b)] by the Pound–Drever–Hall (PDH) approach [26]. The laser frequency noise is measured by the standard short delayed self-heterodyne method (SDSH) [27]. To analyze the noise of the produced Brillouin laser, an unbalanced fiber Mach–Zehnder interferometer (FMZI) is built as a frequency discriminator, so that the frequency fluctuations can be converted and measured through intensity fluctuations. As depicted in Fig. 2, the detected output of the FMZI is further fed into a phase noise analyzer for examining the single-sideband (SSB) phase noise of the beat note signal.

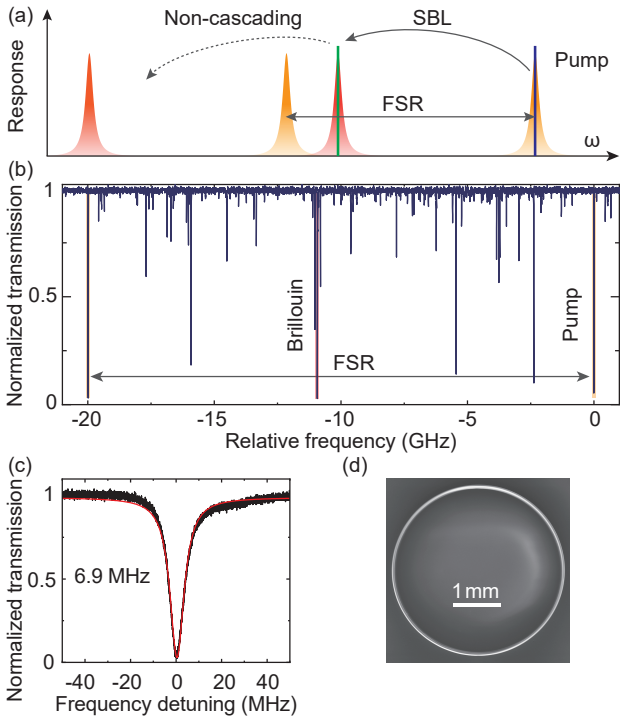

Fig. 1. (a) Spectral diagram for non-cascading Brillouin laser operation. Lorentzian line shapes in different colors indicate different transverse mode families. Phase matching for Brillouin lasing is fulfilled with two optical modes from different transverse mode families so as to prevent cascading. (b) Normalized transmission of Brillouin mode and pump mode, where the frequency span covers a full FSR of the pump mode. (c) Zoom-in view of normalized transmission spectrum of the Brillouin mode with a Lorentz fitting curve (gray line). (d) Scanning electron microscopy (SEM) image of the microtoroid resonator.

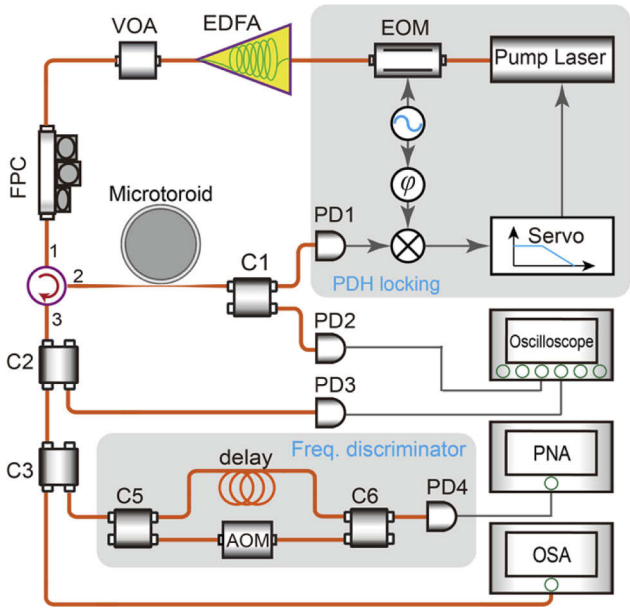

Fig. 2. Experimental setup for generating and characterizing the high-power, low-noise Brillouin microlaser. The pump laser is Pound–Drever–Hall (PDH) locked to the pump mode resonance. The backward-propagating Brillouin laser is separated using a fiber circulator and then delivered to an optical frequency discriminator and an optical spectrum analyzer (OSA) for frequency noise and optical spectrum analysis. EOM, electro-optical modulator (Thorlabs, LN53S-FC); EDFA, erbium-doped fiber amplifier; VOA, variable optical attenuator; FPC, fiber polarization controller; AOM, acoustic optical modulator (Gooch & Housego, T-M080-0.4C2J-3-F2S); PD1–4, photodetectors (PD1–3, Newport, 2053-FC-M; PD4, Newport, 1611FC-AC); C1–6, fiber couplers; PNA, phase noise analyzer (Rohde & Schwarz, FSWP26).

The output Brillouin laser power versus the pump power is reported in Fig. 3, where a threshold power of ~49 mW was recorded. In the power range of 50–100 mW, we found the slope efficiency to be about 83.6% via a linear fitting (not shown). However, if we continued to increase the pump power, a gradual reduction of the pump efficiency was observed and the output Brillouin laser power was eventually saturated at ~126 mW when the pump power was ~320 mW. To the best of our knowledge, this is a remarkable output power record for a chip-based narrow-linewidth microlaser. Also, this achieved output power is larger than the narrow-linewidth fiber Brillouin laser [28]. The inset of Fig. 3 displays a typical optical spectrum in the backward direction in the presence of inevitable scattered pump laser, where the Brillouin frequency shift is ~10.8 GHz.

To have a quantitative understanding of the power saturation-like phenomenon, we model the overall processes by the following set of coupled-mode equations under the rotating-wave approximation [29,30]:

$$\frac{da_1}{dt} = \left(-i\Delta\omega_p + i\beta_1\Delta T - \frac{\gamma_1}{2}\right)a_1 - ig_b a_2 b + \sqrt{\kappa_1}s_{in}, \quad (1)$$

$$\frac{da_2}{dt} = \left(-i\Delta\omega_b + i\beta_2\Delta\, T - \frac{\gamma_2}{2}\right)a_2 - ig_b a_1 b^*, \quad (2)$$

$$\frac{db}{dt} = \left(-i\Delta\Omega_m - \frac{\gamma_m}{2}\right)b - ig_b a_1 a_2^*, \quad (3)$$

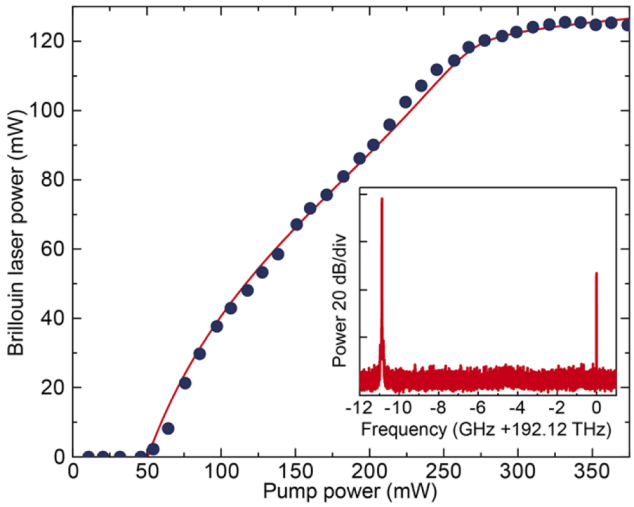

Fig. 3. Measured (dots) and simulated (line) Brillouin laser power versus pump power, where a threshold power of ~49 mW is observed. Inset shows a typical optical spectrum of the Brillouin laser in the presence of a back-scattered pump laser.

$$\frac{d\Delta T}{dt} = -\frac{1}{\tau_T}\Delta T + c_{T,1}|a_1|^2 + c_{T,2}|a_2|^2. \quad (4)$$

Here, a_1, a_2, and b stand for the fields of the intracavity pump, Brillouin, and acoustic modes, respectively; $\Delta\omega_p = \omega_p - \omega_1$, $\Delta\omega_b = \omega_b - \omega_2$, and $\Delta\Omega_m = \Omega_m - \Omega_0$ respectively represent the frequency detunings of the pump, Brillouin, and acoustic waves of frequencies ω_p, ω_b, and Ω_m with respect to their resonant frequencies ω_1, ω_2, and Ω_0; γ_1, γ_2, and γ_m are the decay rates of the pump, Brillouin, and acoustic fields. Additionally, κ_1 denotes the coupling strength between the tapered fiber and the pumped cavity; s_{in} is the amplitude of the input pump field in the fiber; β_1 and β_2 respectively represent the coefficients of thermo-optic-effect induced frequency drifts of the pump and Brillouin modes; τ_T is the thermal relaxation time; $c_{T,1}$ and $c_{T,2}$ stand for the thermal-absorption coefficients of the pump and Brillouin modes, respectively; and g_b is the coupling coefficient between the optical and acoustic modes in the SBS process. The output power of the cavity Brillouin laser can be thus calculated from

$$P_{out} = \kappa_2 |a_2|^2, \tag{5}$$

with κ_2 being the coupling rate between the tapered fiber and the cavity of the Brillouin mode.

We are interested in the steady-state solutions of Eqs. (1)–(4) by setting $da_1/dt = 0$, $da_2/dt = 0$, $db/dt = 0$, and $d\Delta T/dt = 0$. After some algebra, Eqs. (1)–(4) are reduced to

$$\left(-i\Delta\omega_p + i\alpha_1(|a_1|^2 + |a_2|^2) - \frac{\gamma_1}{2}\right) a_1 - \frac{g_b^2}{i\Delta\Omega_m + \frac{\gamma_m}{2}} |a_2|^2 a_1 + \sqrt{\kappa_1} s_{in} = 0, \tag{6}$$

$$\left(-i\Delta\omega_b + i\alpha_2(|a_1|^2 + |a_2|^2) - \frac{\gamma_2}{2}\right) a_2 - \frac{g_b^2}{i\Delta\Omega_m - \frac{\gamma_m}{2}} |a_1|^2 a_2 = 0, \tag{7}$$

where, for simplicity, $c_{T,1} = c_{T,2} = c_T$ is assumed, and $\alpha_1 = \tau_T \beta_1 c_T$ and $\alpha_2 = \tau_T \beta_2 c_T$. To simulate the output Brillouin laser with different input pump powers, we calculate and seek the highest Brillouin laser output power under each pump power with Eqs. (6) and (7). To fit the measured Brillouin laser power in Fig. 3, the theoretical calculation gives $\alpha_1 - \alpha_2 = 2\pi \times 22.8$ kHz/pJ and $\omega_p - \omega_b - \Omega_m = -2\pi \times 78$ MHz. Other measured parameters are $\gamma_1 = 2\pi \times 13.3$ MHz, $\gamma_2 = 2\pi \times 6.9$ MHz, $\kappa_1 = 2\pi \times 7.8$ MHz, $\kappa_2 = 2\pi \times 4.8$ MHz, and $\gamma_m = 2\pi \times 140$ MHz. Here, the γ_m is measured by comparing the frequency noise of the generated Brillouin laser and the pump light when the transferred pump noise dominates [31]. In addition, the coupling coefficient $g_b \approx 2.73 \times 10^{12}$ Hz/J$^{1/2}$ is theoretically derived from the models on the cavity Brillouin gain [14,22]. With the above parameters, we obtained the threshold of the pump power to be approximately 50 mW and the saturation power of the Brillouin laser to be approximately 126 mW. As one can see from Fig. 3, our theoretical curve matches exceedingly well with the experimental data.

Based on the model described above, we attribute the saturation behavior of our Brillouin laser to the interplay between the Brillouin lasing and thermo-optic effect. Theoretically, since the two optical modes in the Brillouin lasing process belong to different families, the strengths of the thermo-optic effect that they experience become different. This in turn gives rise to different spacing between the pump and Brillouin mode resonant frequencies as the growth of the intracavity Brillouin laser power. Such a change will alternatively result in the reduction of the corresponding Brillouin gain. Consequently, the saturation of the Brillouin laser output power will take place.

The performance of the demonstrated Brillouin laser is reported in Fig. 4, which shows the measured fundamental frequency noise at different output Brillouin laser power. During this measurement, the delay fiber is set at ~2.5 km in length for better resolution [27]. To attain the Schawlow–Townes-like (ST-like) fundamental frequency noise evolution of the Brillouin microlaser along with the increase of the output of the Brillouin laser, we use a laser with a narrower linewidth (Toptica CTL1550) as the pump source to minimize the noise coupled from the pump laser. This pump laser has a fundamental frequency noise of approximately 23 Hz^2/Hz at its best performance. In the measurement, the fundamental frequency noise is measured at a range of input pump powers, while the coupling conditions between the fiber taper and the microcavity are fixed. In the meantime, the driven current of the diode is also fixed whereas the pump power is controlled by the variable optical attenuator (VOA), as shown in Fig. 2. The measured results are plotted as dots in Fig. 4(a), where the error bars are standard deviations for five consecutive measurements. As a comparison, we also theoretically calculate the transferred frequency noise from the pump laser, the ST-like frequency noise,

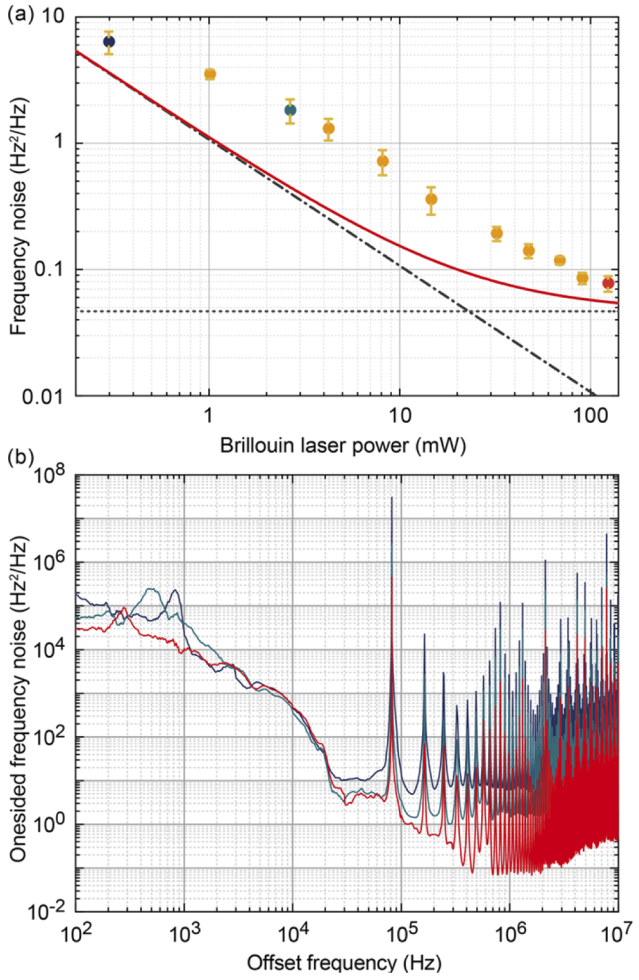

Fig. 4. (a) Measured Brillouin laser fundamental frequency noise with different output Brillouin laser powers (dots). The error bars are standard deviations of five measurements. Transferred noise from the pump laser (dotted line), the theoretical ST-like fundamental frequency noise (dashed line), and the overall fundamental frequency noise (solid line). (b) Measured frequency noise at different pump powers as marked with the corresponding colors in panel (a).

and the overall fundamental frequency noise [31]. Also, due to the backscattered pump being much lower than the generated Brillouin laser (inset of Fig. 3), the frequency noise induced from the backscattered pump can be safely neglected during our measurement. As one can see, the measured fundamental frequency noise clearly exhibits an inverse power dependency. The deviation of the measured values from the theoretical curve may arise from the phase-mismatch-induced linewidth enhancement [32]. In this work, we have achieved the minimum fundamental frequency noise of 78 mHz·Hz/Hz at the maximum output power, corresponding to a fundamental linewidth of 245 mHz.

In summary, we have successfully demonstrated a chip-based Brillouin microlaser with intriguing features of high output power and low noise at the 1550-nm wavelength using a microtoroid resonator. The obtained output power is as high as 126 mW, a record for the chip-based Brillouin microlaser. Of importance, we observed that the laser output power is limited by the thermo-optic-effect-induced mode mismatch with increased pump power. This suggests that the output power can be further enhanced by reducing the thermal nonlinearity in the microresonator via enlarging the mode volume or annealing the sample to lower its thermal absorption. Note that a waveguide-integrated-microtoroid scheme [33] is promising for practical applications. We expect such a high-power Brillouin microlaser will find more practical applications in many areas such as atomic physics, gyroscopes, light detection and ranging (LIDAR), and integrated nonlinear photonics.

Funding. National Key Research and Development Program of China (2021YFA1400803, 2017YFA0303703); National Natural Science Foundation of China (NSFC) (61922040, 12104224); Guangdong Major Project of Basic and Applied Basic Research (2020B0301030009); Zhangjiang Laboratory, Fundamental Research Funds for the Central Universities (021314380189).

Disclosures. The authors declare no conflicts of interest.

Data availability. Data underlying the results presented in this paper are not publicly available at this time but may be obtained from the authors upon reasonable request.

REFERENCES

1. I. S. Grudinin, A. B. Matsko, and L. Maleki, Phys. Rev. Lett. **102**, 043902 (2009).
2. M. Tomes and T. Carmon, Phys. Rev. Lett. **102**, 113601 (2009).
3. B. J. Eggleton, C. G. Poulton, and R. Pant, Adv. Opt. Photonics **5**, 536 (2013).
4. B. J. Eggleton, C. G. Poulton, P. T. Rakich, M. J. Steel, and G. Bahl, Nat. Photonics **13**, 664 (2019).
5. H. Lee, T. Chen, J. Li, K. Y. Yang, S. Jeon, O. Painter, and K. J. Vahala, Nat. Photonics **6**, 369 (2012).
6. J. Li, H. Lee, and K. J. Vahala, Opt. Lett. **39**, 287 (2014).
7. W. Loh, A. A. S. Green, F. N. Baynes, D. C. Cole, F. J. Quinlan, H. Lee, K. J. Vahala, S. B. Papp, and S. A. Diddams, Optica **2**, 225 (2015).
8. S. Gundavarapu, G. M. Brodnik, M. Puckett, T. Huffman, D. Bose, R. Behunin, J. Wu, T. Qiu, C. Pinho, N. Chauhan, J. Nohava, P. T. Rakich, K. D. Nelson, M. Salit, and D. J. Blumenthal, Nat. Photonics **13**, 60 (2019).
9. H. Wang, L. Wu, Z. Yuan, and K. J. Vahala, "Towards milli-Hertz laser frequency noise on a chip," arXiv:2010.09248 (2020).
10. W. Loh, D. Kharas, R. Maxson, G. N. West, A. Medeiros, D. Braje, P. W. Juodawlkis, and R. McConnell, "Cooling of an Integrated Brillouin Laser below the Thermal Limit," arXiv:2112.00846 (2021).
11. N. Chauhan, A. Isichenko, K. Liu, J. Wang, Q. Zhao, R. O. Behunin, P. T. Rakich, A. M. Jayich, C. Fertig, C. W. Hoyt, and D. J. Blumenthal, Nat. Commun. **12**, 4685 (2021).
12. Y.-H. Lai, M.-G. Suh, Y.-K. Lu, B. Shen, Q.-F. Yang, H. Wang, J. Li, S. H. Lee, K. Y. Yang, and K. J. Vahala, Nat. Photonics **14**, 345 (2020).
13. J. Li, H. Lee, and K. J. Vahala, Nat. Commun. **4**, 2097 (2013).
14. Y. Bai, M. Zhang, Q. Shi, S. Ding, Y. Qin, Z. Xie, X. Jiang, and M. Xiao, Phys. Rev. Lett. **126**, 063901 (2021).
15. M. W. Harrington, G. M. Brodnik, T. C. Briles, J. R. Stone, R. H. Streater, S. B. Papp, and D. J. Blumenthal, in *Optical Fiber Communication Conference (OFC)* (2020), paper T4G.6.
16. G. Lin, S. Diallo, K. Saleh, R. Martinenghi, J.-C. Beugnot, T. Sylvestre, and Y. K. Chembo, Appl. Phys. Lett. **105**, 231103 (2014).
17. N. T. Otterstrom, R. O. Behunin, E. A. Kittlaus, Z. Wang, and P. T. Rakich, Science **360**, 1113 (2018).
18. D.-G. Kim, S. Han, J. Hwang, I. H. Do, D. Jeong, J.-H. Lim, Y.-H. Lee, M. Choi, Y.-H. Lee, D.-Y. Choi, and H. Lee, Nat. Commun. **11**, 5933 (2020).
19. R. O. Behunin, N. T. Otterstrom, P. T. Rakich, S. Gundavarapu, and D. J. Blumenthal, Phys. Rev. A **98**, 023832 (2018).
20. M. Asano, Y. Takeuchi, S. K. Ozdemir, R. Ikuta, L. Yang, N. Imoto, and T. Yamamoto, Opt. Express **24**, 12082 (2016).
21. G. Lin and Q. Song, Laser Photonics Rev. **16**, 2100184 (2021).
22. Y. Qin, S. Ding, S. Lei, J. Liu, Y. Bai, M. Zhang, Y. Li, J. Wen, X. Jiang, and M. Xiao, Opt. Lett. **47**, 421 (2022).
23. M. Puckett, D. Bose, K. Nelson, and D. J. Blumenthal, in *Conference on Lasers and Electro-Optics (CLEO)* (2019), paper SM4O.1.
24. J. Ma, X. Jiang, and M. Xiao, Photonics Res. **5**, B54 (2017).
25. K. J. Vahala, Nature **424**, 839 (2003).
26. R. W. P. Drever, J. L. Hall, F. V. Kowalski, J. Hough, G. M. Ford, A. J. Munley, and H. Ward, Appl. Phys. B **31**, 97 (1983).
27. S. Camatel and V. Ferrero, J. Lightwave Technol. **26**, 3048 (2008).
28. J. Geng, S. Staines, Z. Wang, J. Zong, M. Blake, and S. Jiang, IEEE Photonics Technol. Lett. **18**, 1813 (2006).
29. W. Loh, S. B. Papp, and S. A. Diddams, Phys. Rev. A **91**, 053843 (2015).
30. T. Carmon, L. Yang, and K. J. Vahala, Opt. Express **12**, 4742 (2004).
31. J. Li, H. Lee, T. Chen, and K. J. Vahala, Opt. Express **20**, 20170 (2012).
32. Z. Yuan, H. Wang, L. Wu, M. Gao, and K. J. Vahala, Optica **7**, 1150 (2020).
33. X. Zhang and A. M. Armani, Opt. Express **21**, 23592 (2013).